Charged-particle rapidity density in Au+Au collisions in a quark combination model

Feng-lan Shao,[1] Tao Yao,[2] and Qu-bing Xie[2]
[1]*Department of Physics, Qufu Normal University, Shandong 273165, People's Republic of China*
[2]*Department of Physics, Shandong University, Shandong 250100, People's Republic of China*
(Received 11 September 2006; published 14 March 2007)

Rapidity/pseudorapidity densities for charged particles and their centrality, rapidity, and energy dependence in Au+Au collisions at the Relativistic Heavy Ion Collider are studied in a quark combination model. Using a Gaussian-type rapidity distribution for constituent quarks as a result of Landau hydrodynamic evolution, the data at $\sqrt{s_{NN}} = 130, 200$ GeV at various centralities in full pseudorapidity range are well described, and the charged-particle multiplicities are reproduced as functions of the number of participants. The energy dependence of the shape of the $dN_{ch}/d\eta$ distribution is also described at various collision energies $\sqrt{s_{NN}} = 200, 130, 62.4$ GeV in central collisions with same value of parameters except 19.6 GeV. The calculated rapidity distributions and yields for the charged pions and kaons in central Au+Au collisions at $\sqrt{s_{NN}} = 200$ GeV are compared with experimental data of the BRAHMS Collaboration.

DOI: 10.1103/PhysRevC.75.034904 PACS number(s): 13.87.Fh, 12.38.Bx, 12.40.−y

I. INTRODUCTION

The Relativistic Heavy Ion Collider (RHIC) at Brookhaven National Lab was built to search for quark matter or the so-called quark-gluon plasma (QGP). Since its first run in 2000, a huge number of data have been accumulated and a comprehensive analysis of these data has been carried out. A variety of experimental facts from different aspects imply that the strongly coupled QGP has probably been produced in central Au+Au collisions at RHIC. For recent reviews of QGP and summary of experimental data, see e.g. Refs. [1–6]. Central Au+Au collisions are characterized by the production of thousands of charged particles in vacuum. The charged-particle density per unit rapidity or pseudorapidity dN_{ch}/dy or $dN_{ch}/d\eta$ is one of the most important observables to measure for the signal of QGP, from which a lot of information about the hot and dense matter can be extracted [7–13]. One can scale $dN_{ch}/d\eta$ or dN_{ch}/dy by the number of participant nucleon pairs $\langle N_{\rm part}/2\rangle$ and observe its logarithmic increase with $\langle N_{\rm part}\rangle$, which is regarded as an evidence of color glass condensate [8,9,14,15]. From the rapidity/pseudorapidity density and the transverse energy per particle, one can determine via Bjorken method the real density of the fireball, which can provide one piece of evidence for the deconfinement phase transition. The experimental data about the charged-particle rapidity density have been presented by the PHOBOS collaboration [16,17], the PHENIX Collaboration [18], and the BRAHMS Collaboration [19,20].

In this article we will use a quark combination model to study the rapidity/pseudorapidity density varied with the number of participants and the energy in full rapidity range. The quark combination picture is successful in describing many features of multiparticle production in hadronic collisions. In ultrarelativistic heavy-ion collisions at RHIC energies, a lot of new features are found, e.g., the high ratio of $n_p/n_\pi \sim 1$ at intermediate transverse momenta, which supports quark coalescence or recombination picture [21–23]. The quark number scaling of the elliptic flow is also a manifestation of the quark coalescence or recombination [24–26]. In this article we will use a binary potential model for the constituent quark production and then let the constituent quarks combine into initial hadrons according to a quark combination rule. Then we allow the resonances in the initial hadrons to further decay to final hadrons with the help of the event generator PYTHIA 6.3 [27].

The article is organized as follows. In the next section we give a brief description of the model for constituent quark production and combination. In Sec. III, we present our predictions for the rapidity/pseudorapidity densities varied with the number of participants in the full rapidity range at $\sqrt{s_{NN}} = 130, 200$ GeV, the energy dependence of the $dN_{ch}/d\eta$ distribution at various collision energies for central collisions, and the results for the rapidity densities dN/dy and yields for charged pions and kaons in the central collisions at $\sqrt{s_{NN}} = 200$ GeV. The summary and discussions are in Sec. IV.

II. THE QUARK PRODUCTION AND COMBINATION MODEL

In this section we give a brief introduction of the quark production and combination model we use. The model was first proposed for high energy e^+e^- and pp collisions [28–33] and recently extended to ultrarelativistic heavy-ion collisions [34,35]. It has also been applied to the multiparton systems in high energy e^+e^- annihilations [36–39].

A. An effective model for quark production

The quark production from vacuum is a very sophisticated nonperturbative process. The color glass condensate model is a semiclassical QCD effective theory for the quark production in heavy-ion collisions [14,15]. In this article we use a simple model for quark production that is of statistical nature without dynamic details. We determine the number of constituent quarks by the total effective energy for producing quarks from

the vacuum excitation. The effective energy consists of the part for quark static masses and that for effective interquark potentials.

Consider a system of N_q quarks and antiquarks excited in vacuum, the number of light and strange quarks/antiquarks follow the ratio $\mathrm{N}_u : \mathrm{N}_d : \mathrm{N}_s = 1 : 1 : \lambda_s$ with $N_q = N_u + N_d + N_s$, where $\lambda_s < 1$ is the strangeness suppression factor due to the heavier mass of strange quarks/antiquarks. The average quark mass is given by $m = (2m_u + \lambda_s m_s)/(2 + \lambda_s)$, where $m_u = m_d$ is the light quark mass and m_s the strange quark mass.

We assume that the interaction is characterized by an interquark potential V that takes a substantial fraction of total effective energy. The constituent quark number can be determined from the following energy equation,

$$E = \langle N_q \rangle m + \frac{\langle N_q \rangle}{2}(\langle N_q \rangle - 1)\langle V \rangle, \tag{1}$$

which gives the number of constituent quarks as

$$\langle N_q \rangle = 2[(\alpha^2 + \beta E)^{1/2} - \alpha], \tag{2}$$

where

$$\beta \equiv \frac{1}{2\langle V \rangle}, \alpha \equiv \beta m - \frac{1}{4}. \tag{3}$$

Note that the quark number N_q follows a specific distribution, so does the potential, we have taken their averages in the above equations. In Eq. (1), we included only the two-body potential leading to a $E^{1/2} \sim s^{1/4}$ asymptotic behavior for N_q at high energy if $\langle V \rangle$ is constant. For a strong coupling system, it is possible that the n-body ($n > 2$) potential might be more important, and the asymptotic behavior then becomes $N_q \sim s^{1/2n}$. When n is large, N_q more and more approaches a logarithmic increase with energy.

It has been found in the PHOBOS experiments that in the energy range $\sqrt{s_{NN}} \approx$ 20–200 GeV, the total multiplicity per participating nucleon pair ($\langle N_{\mathrm{ch}} \rangle / \langle N_{\mathrm{part}} \rangle$) in central Au+Au collisions scales with $\sqrt{s_{NN}}$ in the same way as $\langle N_{\mathrm{ch}} \rangle$ with $\sqrt{s}$ in e^+e^- collisions, see Fig. 2 of Ref. [40]. This suggests a universal mechanism for particle production in strongly interacting systems at high energies, which is mainly controlled by the amount of effective energy available. The effective energy for high energy AA collisions is found to be approximately just $\sqrt{s_{NN}}$ [40]. In addition, it has also been shown in the PHOBOS experiments that the Au+Au data approximately agree with the scaled pp and $p\overline{p}$ data (an effective energy $\sqrt{s_{\mathrm{eff}}} = \sqrt{s}/2$, which approximately accounts for the "leading particle effect"). The reduction of the leading particle effect in central nuclear collisions compared to $pp/p\overline{p}$ collisions is easy to understand because each participating nucleon is typically struck four to six times on average as it passes through the oncoming gold nucleus in central collisions. Therefore the multiple collisions simultaneously excite and dissociate the participating nucleons, transferring much more of the energy from the forward direction toward midrapidity than found in an average $pp/p\overline{p}$ collision. Based on these experimental facts we extend our quark production model originally applied to e^+e^- annihilation to heavy-ion collisions. The average quark number in nucleus-nucleus collisions can be written as

$$\langle N_q \rangle = 2[(\alpha^2 + \beta\sqrt{s_{NN}})^{1/2} - \alpha]\langle N_{\mathrm{part}}/2 \rangle. \tag{4}$$

Note that the effective energy E is equal to collision energy $\sqrt{s}$ for light quark events in e^+e^- annihilation (but $E \neq \sqrt{s}$ for heavy quark events). In this work, we consider only light quark; therefore, the effective energy is approximately taken to be $E = \sqrt{s_{NN}}$. Here the average number of quarks and antiquarks $\langle N_q \rangle$ includes not only new produced quarks and antiquarks but also some additional quarks left by the incident nuclei.

B. Model for quark combination

In this subsection we briefly summarize how quarks combine into hadrons in our model. In this work, we consider only the production of 36-plets of meson and 56-plets of baryon. Note that all these hadrons after combination are primarily produced; to get the spectra comparable to the data, one has to let them decay in their center-of-mass system. It is well known that all resonance decays are included in decay part of the event generator PYTHIA. Here we make use of the event generator PYTHIA 6.3 [27] to deal with resonance decays. The basic idea is to put N_q quarks and antiquarks line up in a one-dimensional order in phase space, e.g., in rapidity, and let them combine into initial hadrons one by one following a combination rule. See Sec. II of Ref. [34] for short description of such a rule. We note that it is very straightforward to define the combination in one-dimensional phase space, but it is highly complicated to do it in two- or three-dimensional phase space [41]. The flavor SU(3) symmetry with strangeness suppression in the yields of initially produced hadrons is fulfilled in the model [28,30]. Using the model, we have described most of multiplicity data for hadrons in electron-positron and proton-proton/antiproton collisions [28–33]. Also we solved a difficulty facing other quark combination models in describing the TASSO data for baryon-antibaryon correlation in electron-positron collisions [33]. Combined with the color flow picture [37], the model can describe the hadroniztion of multiparton states [36,38,39]. We have extended the model to reproduce the recent RHIC data for hadron multiplicity ratios, p_T spectra [34], and elliptic flows [35] in the central rapidity region.

III. RAPIDITY AND PSEUDORAPIDITY DENSITIES

In this section, we use our combination model to compute the centrality dependence of distributions of rapidity/pseudorapidity densities in Au+Au collisions at $\sqrt{s_{NN}} =$ 130, 200 GeV, study the energy dependence of the shape of the $dN_{\mathrm{ch}}/d\eta$ distribution at various collision energies $\sqrt{s_{NN}} =$ 19.6, 62.4, 130, and 200 GeV for central collisions, and calculate the rapidity densities dN/dy and yields for charged pions and kaons in the central collisions at $\sqrt{s_{NN}} = 200$ GeV.

First we have to fix the parameters of the model. There are two parameters: m and $\langle V \rangle$ or α and β in Eq. (2). As we pointed out, these quarks and antiquarks are constituent, so we use constituent masses $m_u = m_d = 0.34$ GeV and $m_s = 0.5$ GeV, giving the average mass $m = 0.36$ GeV. The

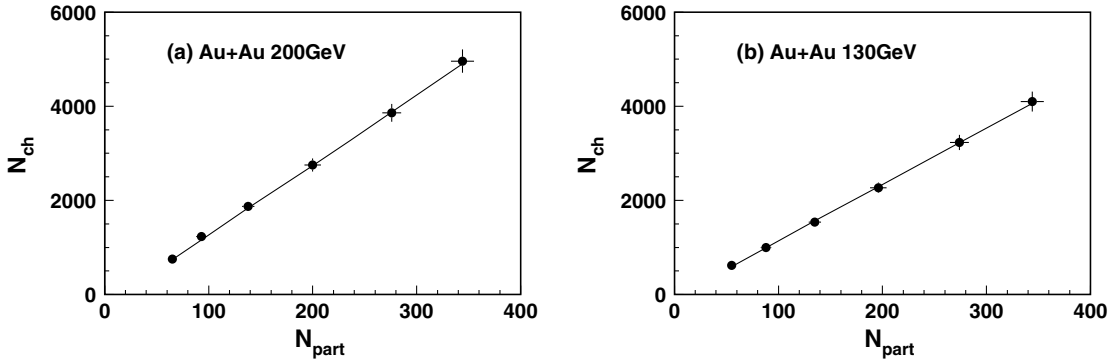

FIG. 1. The centrality-dependent multiplicities of charged particles in Au+Au collisions at $\sqrt{s_{NN}} = 130$, 200 GeV. The solid lines are our results. The data are taken from PHOBOS [17].

strangeness suppression factor is chosen to be $\lambda_s = 0.55$ by fitting the data at RHIC energies [34]. The parameter β is set to 3.6 GeV^{-1}, which described the e^+e^- data. The parameters controlling the total multiplicity are the number of quarks and that of antiquarks. In electron-positron and proton-antiproton collisions, the number of quarks is equal to that of antiquarks, i.e., there are no excess baryons in contrast to antibaryons. For nucleus-nucleus collisions, however, there are some excess baryons deposited by the colliding nuclei. The total number of quarks and antiquarks $\langle N_q \rangle$ is given by Eq. (4). The number of net quarks can be further determined by the ratio of antiproton to proton [34]. At 130 and 200 GeV, we find that the net quark numbers are about 420 and 360, respectively.

With these parameters, we calculate the centrality-dependent multiplicities of charged particles at $\sqrt{s_{NN}} =$ 130, 200 GeV. The results are shown in Fig. 1 and agree with data very well.

To compute the distribution of rapidity/pseudorapidity densities with both energy and centrality dependence, we have to know the rapidity distribution of quarks and antiquarks before hadronization.

In the initial state, colliding nuclei are highly Lorentz contracted along the beam direction. After the initial compression phase, the evolution of highly excited, and possibly deconfined, strongly interacting quark matter can be described by the ideal relativistic hydrodynamics. Under the assumption of full stopping and isentropic expansion, the amount of entropy (dS) contained within the (fluid) rapidity element dy in the Landau hydrodynamic picture is given by [42–46],

$$\frac{dS}{dy} = -\pi R^2 l s_0 \beta c_s \exp(\beta\omega_f)\left[I_0(q) - \frac{\beta\omega_f}{q} I_1(q)\right], \quad (5)$$

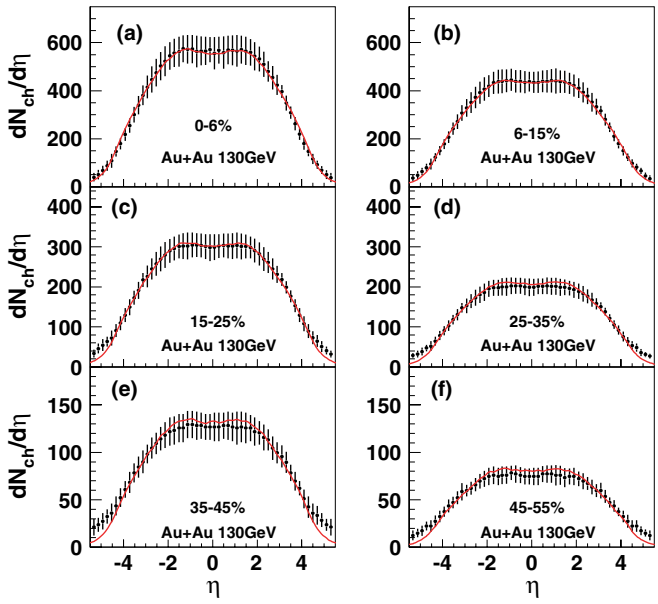

FIG. 2. (Color online) Distributions of pseudorapidity density for charged particles in Au+Au collisions at $\sqrt{s_{NN}} = 130$ GeV for six centrality bins. The solid lines are our results. The data are taken from PHOBOS [17].

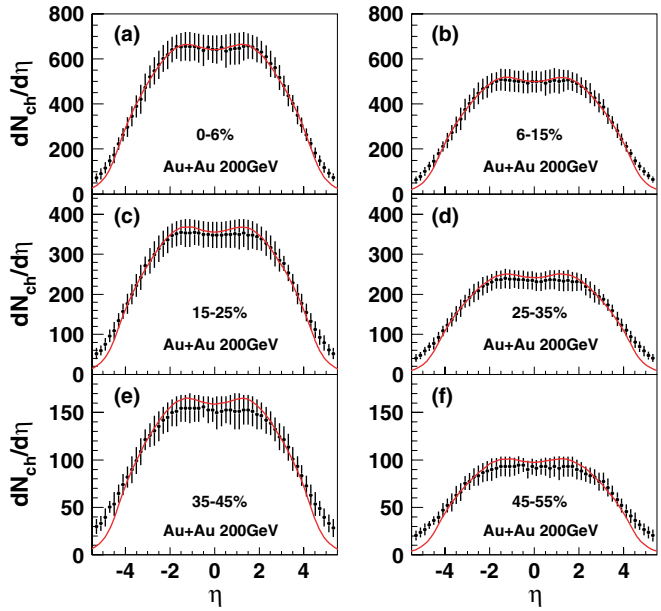

FIG. 3. (Color online) Same as in Fig. 2 but at $\sqrt{s_{NN}} = 200$ GeV.

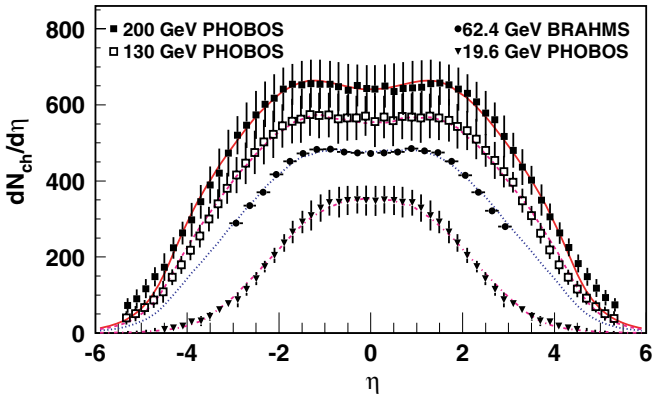

FIG. 4. (Color online) Pseudorapidity densities $dN/d\eta$ for charged particles in most central collisions at various collision energies $\sqrt{s_{NN}} = 19.6, 62.4, 130, 200$ GeV. The lines are our results. The PHOBOS data are from Ref. [17], whereas the BRAHMS data are from Ref. [52].

where $2\beta \equiv (1-c_s^2)/c_s^2$ and $q \equiv \sqrt{\omega_f^2 - c_s^2 y^2}$ with $c_s^2 = (\frac{\partial P}{\partial \epsilon})_{\text{isentropic}}$ the sound velocity square. ω_f is related to the initial and freeze-out temperature T_f and T_0 by $\omega_f \equiv \ln(T_f/T_0)$. R is the radius of the nuclei. $2l$ is the initial longitudinal length. s_0 is the initial entropy density. I_0 and I_1 are the Bessel functions. The quantity $\pi R^2 l s_0$ is fixed to normalize the experimental data at midrapidity. For $|\omega_f| \gg c_s y$ the quantity dS/dy can be approximated by a Gaussian distribution,

$$\frac{dS}{dy} \sim \frac{\exp(-\frac{y^2}{2\sigma^2})}{\sqrt{2\pi\sigma^2}}, \tag{6}$$

where

$$\sigma^2 = \frac{2|\omega_f|}{1-c_s^2} \approx \frac{2c_s^2}{1-c_s^4} \ln\left(\frac{s_{NN}}{2m_p m_\pi}\right), \tag{7}$$

where m_p is proton mass and m_π is pion mass, taken $T_f \approx m_\pi$. There is only one parameter c_s^2 left to be determined by experiments. dS/dy is proportional to dN/dy [47]. Therefore, the rapidity distribution for quarks and antiquark before hadronization can be written as

$$\frac{dN}{dy} \sim \exp\left(-\frac{y^2}{2\sigma^2}\right). \tag{8}$$

It is known that collisions at RHIC are neither fully stopped nor fully transparent. In Ref. [48] the BRAHMS Collaboration have measured the charged meson rapidity distributions in central Au+Au collisions at $\sqrt{s_{NN}} = 200$ GeV and specially studied the applicable extent of Eq. (8) at RHIC. They have found that the rapidity distributions of pions are in surprisingly good agreement with a hydrodynamic model based on the Landau expansion picture except around $y = 0$; see Fig. 4 of Ref. [48]. Recently, many studies have applied the Landau hydrodynamic model to RHIC; see, for example, Refs. [49–51]. In this article, we will use Eq. (8) to the constituent quarks and antiquarks level before hadronization and study rapidity/pseudorapidity distributions for charged particles and their centrality and energy dependence in Au+Au collisions at RHIC in a quark combination model.

We take the sound velocity square $c_s^2 = 1/4$ for QGP before hadronization ($c_s^2 = 1/3$ for ideal gas). We have used the fact that all quarks and anti-quarks are within the rapidity range $y \in [-4.2, 4.2]$ at 130 GeV and 200 GeV at all centralities of collisions.

With this input, we give $dN_{ch}/d\eta$ as functions of η at all available centralities at $\sqrt{s_{NN}} = 130, 200$ GeV. The results are shown in Fig. 2 and Fig. 3. One can see a good agreement between our model predictions and data in central collisions. For peripheral collisions, there is a slight deviation from the data. The tails at large pseudorapidities especially in peripheral collisions are associated with remnants of collision spectators from the incoming nuclei. Therefore, our results are slightly lower than the data. Now we study the energy dependence of the shape of the η distribution of charged particles at various energies of Au+Au collisions. We compute pseudorapidity densities in full pseudorapidity range in most central collisions at $\sqrt{s_{NN}} = 62.4$ GeV and compare with BRAHMS data [52]. Here, the quark rapidity range is also $y \in [-4.2, 4.2]$ and the sound velocity square is also $c_s^2 = 1/4$ same as in 130 and 200 GeV. By studying we find that the shape of η distribution is mainly determined by the energy and the sound velocity and the the quark rapidity region only influences the forward pseudorapidity. The quark rapidity range is possibly dependent on the collision energy but not sensitive to that. The calculation results show that there is the same value of the sound velocity for QGP in different collision energies. This indicates a certain kind of universality for the quark matter produced in heavy-ion collisions at the late stage of evolution (before hadronization) at collision energies from 62.4 to 200 GeV. We also studied the results at 19.6 GeV. We find that the model predictions disagree with the data using the constant value of the sound velocity square $c_s^2 = 1/4$ no matter how the quark rapidity region is chosen. We have to set the sound velocity $c_s^2 = 1/7$ and quark rapidity range $y \in$

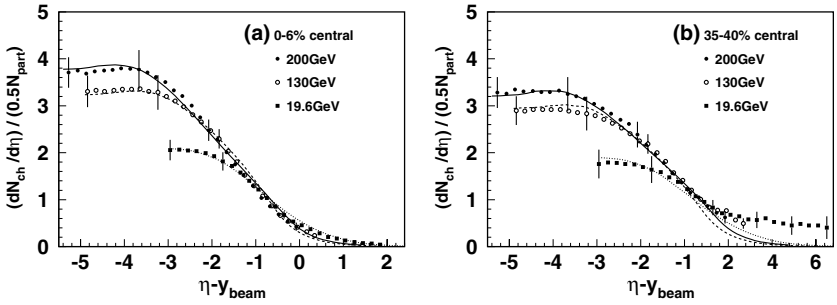

FIG. 5. The scaled, shifted pseudorapidity rapidity density at $\sqrt{s_{NN}} = 19.6, 130$, and 200 GeV. The results at two centrality bins are presented: 0–6% and 35–40%. The lines are our results. The data are from Ref. [17].

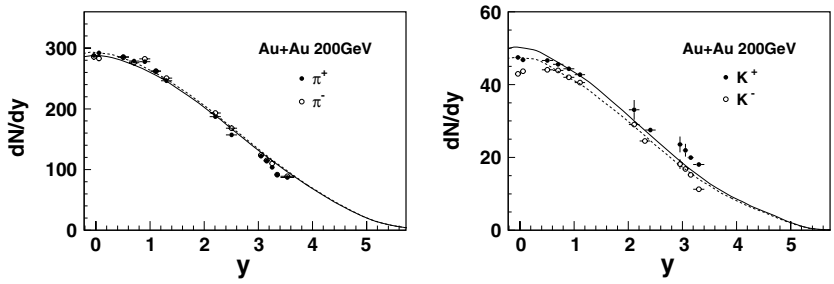

FIG. 6. dN/dy in the 0–5% most central collisions at $\sqrt{s_{NN}} = 200$ GeV. The solid lines are π^+ and K^+, and dashed lines are π^- and K^-. The data are given by BRAHMS Collaborations [48].

$[-3.2, 3.2]$. The change in the sound velocity might reflect the different properties of the matter produced at 19.6 GeV and at 62.4 GeV or higher energies. The model predictions are shown in Fig. 4 at $\sqrt{s_{NN}} = 19.6, 62.4, 130, 200$ GeV. The agreement with data is also satisfactory, which means that our model captures the energy behavior in the available collision energies.

To separate the trivial kinematic broadening of the $dN_{ch}/d\eta$ distribution from the more interesting dynamics, we also study the scaled, shifted pseudorapidity distribution $dN_{\rm ch}/d\eta'/\langle N_{\rm part}/2\rangle$, where $\eta' = \eta - y_{\rm beam}$, for Au+Au collisions at different energies. The calculation results are shown in Fig. 5 at $\sqrt{s_{NN}} = 19.6, 130, 200$ GeV and two centrality bins 0–6% and 35–40%. In most central collisions our model can describe the limit fragmentation very well. But in peripheral collisions there is a disagreement close to beam rapidity. The reason is that in peripheral collisions the beam rapidity region is dominated by spectators and is not covered by our model.

In ultrarelativistic heavy-ion collisions at RHIC energies, charged pions and kaons are copiously produced. The yields of these light mesons carry the information on the entropy and strangeness created in the reactions. Here, we calculate the rapidity density dN/dy and yields of charged pions and kaons in full rapidity for central Au+Au collisions (0–5%) at $\sqrt{s_{NN}} = 200$ GeV. The yields of charged pions and kaons compared with BRAHMS data [48] are shown in Table I. The results for rapidity density distributions of charged pions and kaons are shown in Fig. 6. Here, the pion yields are collected excluding the contributions of hyperon (Λ) and kaon K_{0s} decays. One can see that our model can well describe rapidity densities dN/dy and yields of charged pions and kaons in the whole rapidity range for central Au+Au collisions at $\sqrt{s_{NN}} = 200$ GeV.

Our results show that the rapidity spectra of charged hadrons are almost flat in mid-rapidity, different from the Gaussian distubution of quarks given in Eq. (8). There are two main reasons for the difference. First, in the quark combination model, the rapidity distributions of directly produced light hadrons are different from those of quarks. For example, for π^+ ($u\bar{d}$), the total mass of constituent quarks ($\sim$0.68 GeV) is much larger than its mass ($\sim$0.139 GeV). Due to longitudinal momentum conservation during the combination process, the mass loss is transfered to its kinetic energy leading to the increase of longitudinal velocity β of the pion and therefore that of the pion's rapidity. The shift in rapidity is obvious in the midrapidity region. For heavier hadrons, e.g., ρ^+, whose masses are almost the same as the total mass of the constituent quarks, the rapidity distributions of hadrons are close to the Gaussian distribution of quarks. Second, the mass loss of unstable mother particles will be converted into the kinetic energy of their daughters in their decays, thus the spectrum widths of daughter particles become wider than those of mother particles. We take $\rho^+ \to \pi^+\pi^0$ as an example. The mass of ρ^+ is about 0.769 GeV, larger than the mass of two pions ($\sim$0.279 GeV), therefore the rapidity distribution of the pion from ρ^+ decay is a little broader than that of ρ^+. We compute the rapidity spectra of directly produced π^+, ρ^+ and π^+ from ρ^+ decay. The results are shown in Fig. 7. One can see that the spectrum of directly produced π^+ is slightly lower in midrapidity, whereas that of directly produced ρ^+ almost agrees with the Gaussian distribution. The spectrum of π^+ from ρ^+ decay is slightly lower than that of ρ^+ in midrapidity, as mentioned above. Hence, one sees that with the contribution from ρ^+ decay, the rapidity spectrum of π^+ deviates from the Gaussian shape.

TABLE I. Yields of charged pions and kaons compared with BRAHMS data at 200 GeV [48].

	Data	Our model
π^+	$1660 \pm 15 \pm 133$	1676
π^-	$1683 \pm 16 \pm 135$	1680
K^+	$286 \pm 5 \pm 23$	280
K^-	$242 \pm 4 \pm 19$	242

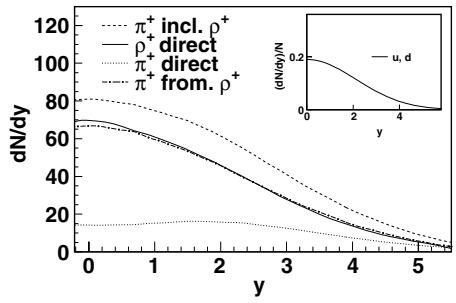

FIG. 7. dN/dy in the 0–5% most central collisions at $\sqrt{s_{NN}} = 200$ GeV. The inset plot shows the $u(d)$ quark. The dotted line is directly produced π^+, the solid line is directly produced ρ^+, dotted-dashed is π^+ from ρ^+ decay and the dashed line is π^+ including ρ^+ decay.

IV. SUMMARY AND DISCUSSIONS

We studied in a combination model the rapidity and pseudorapidity densities at various collision energies and centralities. We used the Landau relativistic hydrodynamic model to describe the the evolution of highly excited and possibly deconfined quark matter. As a result, we obtained the Gaussian-type rapidity spectra of constituent quarks before hadronization. Then we used our combination model to describe the hadronization of initially produced hadrons including resonances, whose decays are dealt with by the event generator PYTHIA 6.3 [27]. We compute charged multiplicities and pseudorapidity densities at a variety of centralities at 130 and 200 GeV. The results for pseudorapidity densities are in good agreement with data in central collisions. In peripheral collisions, our predictions are slightly lower than data due to the fact that our model does not include the influence of the spectators. Our model can well describe the dependence of pseudorapidity densities and charged multiplicities on centralities and the number of participants, respectively. We also calculated pseudorapidity densities at 19.6 and 62.4 GeV that describes the RHIC data very well. This means that our model can reproduce the collision energy dependence of pseudorapidity densities. However, we found that the value of the sound velocity square $c_s^2 = 1/7$ at 19.6 GeV is different from that at 62.4 GeV or higher energies. This imply that there is large change in properties of the hot and dense matter produced at collision energy between 19.6 and 62.4 GeV. To separate the trivial kinematic broadening of the distributions of the pseudorapidity density from more interesting dynamics, we computed the scaled and shifted pseudorapidity density distributions $dN_{\rm ch}/d\eta'/(N_{\rm part}/2)$ with $\eta' = \eta - y_{\rm beam}$ at collision energies 19.6, 130, and 200 GeV. The good agreement with data is found except in the beam rapidity range of peripheral collisions, where our predictions are lower than data. Finally, we present our results for rapidity densities of charged pions and kaons in most central collisions at 200 GeV. No contradiction to data is found. Note that the BRAHMS pion data do not include the decay products of K_s^0 and Λ, we also make the same corrections.

Note added in proof. During the production process of the paper, we became aware of two related papers [references to hep-ph/0410324, hep-ph/0510191] that consider multihadron production with a similar approach.

ACKNOWLEDGMENTS

The authors thank Q. Wang, S.-Y. Li, and Z.-T. Liang for helpful discussions. The work is supported in part by the National Natural Science Foundation of China under the grant 10475049, the foundation of University Doctorate Educational Base of Ministry of Education under the grant 20030422064, and the science fund of Qufu Normal University.

[1] J. Adams *et al*. (STAR Collaboration), Nucl. Phys. **A757**, 102 (2005).
[2] M. Gyulassy and L. McLerran, Nucl. Phys. **A750**, 30 (2005).
[3] P. Jacobs and X. N. Wang, Prog. Part. Nucl. Phys. **54**, 443 (2005).
[4] P. F. Kolb and U. W. Heinz, in *Quark Gluon Plasma 3*, edited by R. C. Hwa and X. N. Wang (World Scientific, Singapore, 2004), pp. 634–714.
[5] P. Braun-Munzinger, K. Redlich, and J. Stachel, in *Quark Gluon Plasma 3*, edited by R. C. Hwa and X. N. Wang (World Scientific, Singapore, 2004), pp. 491–599.
[6] D. H. Rischke, Prog. Part. Nucl. Phys. **52**, 197 (2004).
[7] X. N. Wang and M. Gyulassy, Phys. Rev. Lett. **86**, 3496 (2001).
[8] D. Kharzeev and M. Nardi, Phys. Lett. **B507**, 121 (2001).
[9] D. Kharzeev and E. Levin, Phys. Lett. **B523**, 79 (2001).
[10] A. Capella and D. Sousa, Phys. Lett. **B511**, 185 (2001).
[11] J. Dias de Deus and R. Ugoccioni, Phys. Lett. **B494**, 53 (2000).
[12] K. J. Eskola, K. Kajantie, P. V. Ruuskanen, and K. Tuominen, Nucl. Phys. **B570**, 379 (2000).
[13] K. J. Eskola, K. Kajantie, P. V. Ruuskanen, and K. Tuominen, Phys. Lett. **B543**, 208 (2002).
[14] L. D. McLerran and R. Venugopalan, Phys. Rev. D **49**, 2233 (1994).
[15] R. Venugopalan, Eur. Phys. J. C **43**, 337 (2005).
[16] B. B. Back *et al*. (PHOBOS Collaboration), Phys. Rev. Lett. **85**, 3100 (2000).
[17] B. B. Back *et al*. (PHOBOS Collaboration), Phys. Rev. Lett. **91**, 052303 (2003); **87**, 102303 (2001).
[18] K. Adcox *et al*. (PHENIX Collaboration), Phys. Rev. Lett. **86**, 3500 (2001).
[19] I. G. Bearden *et al*. (BRAHMS Collaborations), Phys. Lett. **B523**, 227 (2001).
[20] I. G. Bearden *et al*. (BRAHMS Collaboration), Phys. Rev. Lett. **88**, 202301 (2002).
[21] R. J. Fries, B. Muller, C. Nonaka, and S. A. Bass, Phys. Rev. Lett. **90**, 202303 (2003).
[22] V. Greco, C. M. Ko, and P. Levai, Phys. Rev. Lett. **90**, 202302 (2003); Phys. Rev. C **68**, 034904 (2003).
[23] R. C. Hwa and C. B. Yang, Phys. Rev. C **67**, 034902 (2003).
[24] S. A. Voloshin, Nucl. Phys. **A715**, 379 (2003).
[25] D. Molnar and S. A. Voloshin, Phys. Rev. Lett. **91**, 092301 (2003).
[26] Z. w. Lin and C. M. Ko, Phys. Rev. Lett. **89**, 202302 (2002); V. Greco and C. M. Ko, Phys. Rev. C **70**, 024901 (2004).
[27] T. Sjostrand, P. Eden, C. Friberg, L. Lonnblad, G. Miu, S. Mrenna, and E. Norrbin, Comput. Phys. Commun. **135**, 238 (2001).
[28] Q. B. Xie and X. M. Liu, Phys. Rev. D **38**, 2169 (1988).
[29] Z.-T. Liang and Q.-B. Xie, Phys. Rev. D **43**, 751 (1991).
[30] Q. Wang and Q. B. Xie, J. Phys. G **21**, 897 (1995).
[31] J. Q. Zhao, Q. Wang, and Q. B. Xie, Sci. Sin. A **38**, 1474 (1995).
[32] Q. Wang, Z. G. Si, and Q. B. Xie, Int. J. Mod. Phys. A **11**, 5203 (1996).
[33] Z. G. Si, Q. B. Xie, and Q. Wang, Commun. Theor. Phys. **28**, 85 (1997).
[34] F. l. Shao, Q. b. Xie, and Q. Wang, Phys. Rev. C **71**, 044903 (2005).
[35] T. Yao, Q. b. Xie, and F. l. Shao, arXiv:nucl-th/0606033.
[36] Q. Wang and Q. B. Xie, Phys. Rev. D **52**, 1469 (1995).
[37] Q. Wang, Q. B. Xie, and Z. G. Si, Phys. Lett. **B388**, 346 (1996).

[38] Q. Wang, G. Gustafson, and Q. B. Xie, Phys. Rev. D **62**, 054004 (2000).
[39] Q. Wang, G. Gustafson, Y. Jin, and Q. B. Xie, Phys. Rev. D **64**, 012006 (2001).
[40] B. B. Back *et al*. (PHOBOS Collaboration), arXiv:nucl-ex/0301017.
[41] M. Hofmann, M. Bleicher, S. Scherer, L. Neise, H. Stocker, and W. Greiner, Phys. Lett. **B478**, 161 (2000).
[42] L. D. Landau, Izv. Akad. Nauk SSSR Ser. Fiz. **17**, 51 (1953).
[43] S. Z. Belenkij and L. D. Landau, Usp. Fiz. Nauk **56**, 309 (1955); Nuovo Cimento Suppl. **3**, 15 (1956).
[44] B. Mohanty and J. Alam, Phys. Rev. C **68**, 064903 (2003).
[45] D. K. Srivastava, J. Alam, S. Chakrabarty, S. Raha, and B. Sinha, Phys. Lett. **B278**, 225 (1992).
[46] D. K. Srivastava, J. e. Alam, S. Chakrabarty, B. Sinha, and S. Raha, Ann. Phys. **228**, 104 (1993).
[47] B. Mohanty, J. Alam, and T. K. Nayak, Phys. Rev. C **67**, 024904 (2003).
[48] I. G. Bearden *et al*. (BRAHMS Collaboration), Phys. Rev. Lett. **94**, 162301 (2005).
[49] P. Steinberg, J. Phys. G **30**, S683 (2004).
[50] M. Murray, J. Phys. G **30**, S667 (2004).
[51] H. Petersen and M. Bleicher, arXiv:nucl-th/0611001.
[52] P. Staszel (for BRAHMS Collaboration), Nucl. Phys. **A774**, 77 (2006).
[53] E. K. G. Sarkisyan and A. S. Sakharov, arXiv:hep-ph/0410324.
[54] E. K. G. Sarkisyan and A. S. Sakharov, arXiv:hep-ph/0510191.